Oncogene (2019) 38:6850–6866
https://doi.org/10.1038/s41388-019-0926-z

ARTICLE

circKDM4C suppresses tumor progression and attenuates doxorubicin resistance by regulating miR-548p/PBLD axis in breast cancer

Yiran Liang[1] · Xiaojin Song[1] · Yaming Li[1] · Peng Su[2] · Dianwen Han[1] · Tingting Ma[1] · Renbo Guo[3] · Bing Chen[4] · Wenjing Zhao[4] · Yuting Sang[1] · Ning Zhang[1] · Xiaoyan Li[1] · Hanwen Zhang[1] · Ying Liu[1] · Yi Duan[1] · Lijuan Wang[4] · Qifeng Yang[1,4]

Received: 1 January 2019 / Revised: 7 July 2019 / Accepted: 23 July 2019 / Published online: 12 August 2019

Abstract

Increasing evidence has indicated that circular RNAs (circRNAs) play a critical role in cancer development. However, only a small number of circRNAs have been experimentally validated and functionally annotated. In this study, using a high-throughput microarray assay, we identified a novel circRNA, circKDM4C, which was downregulated in breast cancer tissues with metastasis. Furthermore, we analyzed a cohort of breast cancer patients and found that circKDM4C expression was decreased in breast cancer tissues, and lower circKDM4C expression was associated with poor prognosis and metastasis in breast cancer. Functionally, we demonstrated that circKDM4C significantly repressed breast cancer proliferation, metastasis, and doxorubicin resistance in vitro and in vivo. Mechanistically, using a dual-luciferase activity assay and AGO2 RNA immunoprecipitation, circKDM4C was identified as a miR-548p sponge. We also found that PBLD was a direct target of miR-548p, which functioned as a tumor suppressor in breast cancer. Moreover, miR-548p overexpression was able to reverse the circKDM4C-induced attenuation of malignant phenotypes and elevated expression of PBLD in breast cancer cells. Taken together, our data indicate that circKDM4C might have considerable potential as a prognostic biomarker in breast cancer, and support the notion that therapeutic targeting of circKDM4C/miR-548p/PBLD axis may be a promising treatment approach for breast cancer patients.

Introduction

Breast cancer is one of the most commonly diagnosed and life-threatening malignant tumors among women worldwide [1]. Despite improvements in the diagnosis and therapeutic strategies of this disease, the prognosis of breast cancer patients is not satisfactory, predominantly due to the high frequency of metastasis and chemoresistance [2–5]. Therefore, better understanding of critical signaling pathways and the discovery of novel therapeutic targets are urgently needed to improve the prognosis of breast cancer patients.

Circular RNAs (circRNAs) were first misinterpreted as products of splicing errors [6]. However, with advances in high-throughput sequencing and bioinformatic analysis, thousands of circRNAs have been identified and found to play important roles in multiple cell types. CircRNAs are generated by the nonsequential back-splicing of pre-mRNA transcripts [7, 8] to form covalently closed continuous loops, which render circRNAs more stable than liner transcripts and insusceptible to RNase R. In addition, evidence has shown that certain circRNAs are more abundant than cognate mRNAs [9]. Due to their stability and abundance [10], circRNAs are conserved across species and may act as better biomarkers for human diseases [11].

Supplementary information The online version of this article (https://doi.org/10.1038/s41388-019-0926-z) contains supplementary material, which is available to authorized users.

✉ Qifeng Yang
qifengy_sdu@163.com

[1] Department of Breast Surgery, Qilu Hospital of Shandong University, Jinan, Shandong 250012, PR China

[2] Department of Pathology, Qilu Hospital of Shandong University, Jinan, Shandong 250012, PR China

[3] Department of Urology, Shandong cancer hospital affiliated to Shandong University, Jinan, Shandong 250117, PR China

[4] Pathology Tissue Bank, Qilu Hospital of Shandong University, Jinan, Shandong 250012, PR China

Some circRNAs have been detected in the cytoplasm and act as miRNA sponges to participate in gene regulation [12, 13]. They also have a critical role in human diseases, especially cancers, as either oncogenes or tumor suppressor genes via different targets in different cancers or different stages [14]. CiRS-7 is one of the most well-known circRNAs, which can serve as a miR-7 sponge and regulate the expression of several oncogenes in different cancers [15–17]. Moreover, circHIPK3 has been shown to act as either a tumor suppressor or an oncogene in different cancers through various signaling pathways [18–21].

In the present study, we identified a novel circRNA derived from the KDM4C gene, termed circKDM4C, as a tumor suppressor in breast cancer. The expression of circKDM4C was significantly downregulated in breast cancer, and negatively associated with breast cancer progression and chemoresistance by regulating the miR-548p activity. Our findings suggested that circRNAs may exert regulatory functions in breast cancer and may be a potential target for breast cancer therapy.

Results

CircKDM4C expression is decreased in breast cancer and correlated with the prognosis of breast cancer patients

To explore the roles of circRNAs in the development of breast cancer, circRNA expression in breast cancer tissues with or without metastasis was explored using microarray analysis. The results showed that 51 circRNAs were significantly differentially expressed with a fold change > 1.5 and $P < 0.05$ (Table S1). Hierarchical clustering showed the ten most increased and decreased circRNAs (Fig. 1a). In addition, the expression of circKDM4C in breast cancer tissues with lymph node metastasis was decreased (Fig. 1b), and lower expression of circKDM4C was associated with a worse overall survival rate (Fig. 1c). CircKDM4C was lower in breast cancer tissues than in matched adjacent normal tissue (Fig. 1d) and was lower in breast cancer cells than in normal breast cells (MCF10A) (Fig. 1e). Moreover, the expression of circKDM4C was higher in cells with lower metastatic abilities (such as MCF-7) compared with cells with higher metastatic abilities (such as MDA-MB-231), which further verifies the negative association between the expression of circKDM4C and the metastatic ability of breast cancer cells.

According to the circBase database, circKDM4C (hsa_circ_0001839) arose from the KDM4C gene on chr9: 6,880,011-6,893,232 and ultimately formed the mature sequence with a length of 292 nt; and we validated the putative circKDM4C junction by Sanger sequencing (Fig. 1f). Moreover, circKDM4C was more resistant to RNase R than linear KDM4C (Fig. 1g), and the half-life of circKDM4C was longer than that of linear KDM4C (Fig. 1h). Subsequently, we designed convergent and divergent primers to amplify circKDM4C and actin. Using cDNA and gDNA from MDA-MB-231 and MCF-7 cells as templates, the convergent primers could amplify both circKDM4C and actin. However, the divergent primers could amplify only circKDM4C using cDNA templates, but not gDNA templates (Fig. 1i). Together, these results demonstrate that circKDM4C is downregulated in breast cancer cells and breast cancer tissues; and that lower circKDM4C expression is associated with a poor prognosis in breast cancer patients.

CircKDM4C inhibits the progression of breast cancer cells in vitro

In an attempt to investigate the biological functions of circKDM4C in breast cancer cells, we designed interference sequences targeting the junction sites of circKDM4C (Fig. 2a). These siRNAs significantly decreased the expression of circKDM4C, but had no effect on its linear isoform (Figs. 2b and S1a). Cell proliferation was measured by MTT and EdU assays, and cell viability was increased by circKDM4C knockdown (Figs. 2c, d and S1b). Then, flow cytometry analysis was performed to evaluate whether circKDM4C affects the cell cycle profile and apoptosis. CircKDM4C knockdown promoted the progression of the cell cycle, as indicated by the fact that fewer cells were distributed in G1 phase and more cells were distributed in S phase (Fig. 2e); circKDM4C knockdown also led to a decreased apoptotic rate (Fig. 2f). Consistently, western blot analysis showed that circKDM4C knockdown could lead to decreased expression of p53, Rb, and p21 (inhibitors of cell cycle progression), but increased expression of CDK4, CDK6, and cyclin D1 (major regulators of G1/S cell cycle checkpoint control) (Fig. 2g). Moreover, transwell analysis demonstrated that circKDM4C knockdown led to increased migration and invasion capabilities in breast cancer cells, which was in accordance with the wound healing assay results (Figs. 2h, i and S1c, d). Subsequently, the tube formation ability of human umbilical vein endothelial cells (HUVECs) was enhanced by treatment with conditioned media (CM) from cells transfected with siRNAs against circKDM4C (Fig. 2j). Given the essential role of epithelial–mesenchymal transition (EMT) in the invasion and migration of cancer cells, we further evaluated the influence of circKDM4C on EMT. Moreover, western blot analysis also demonstrated that circKDM4C knockdown could decrease the expression of epithelial markers and increase the expression of mesenchymal markers (Fig. 2k), highlighting the significant role of circKDM4C in regulating EMT in breast cancer cells. At the morphologic level, circKDM4C-overexpressed cells presented a round-like morphology,

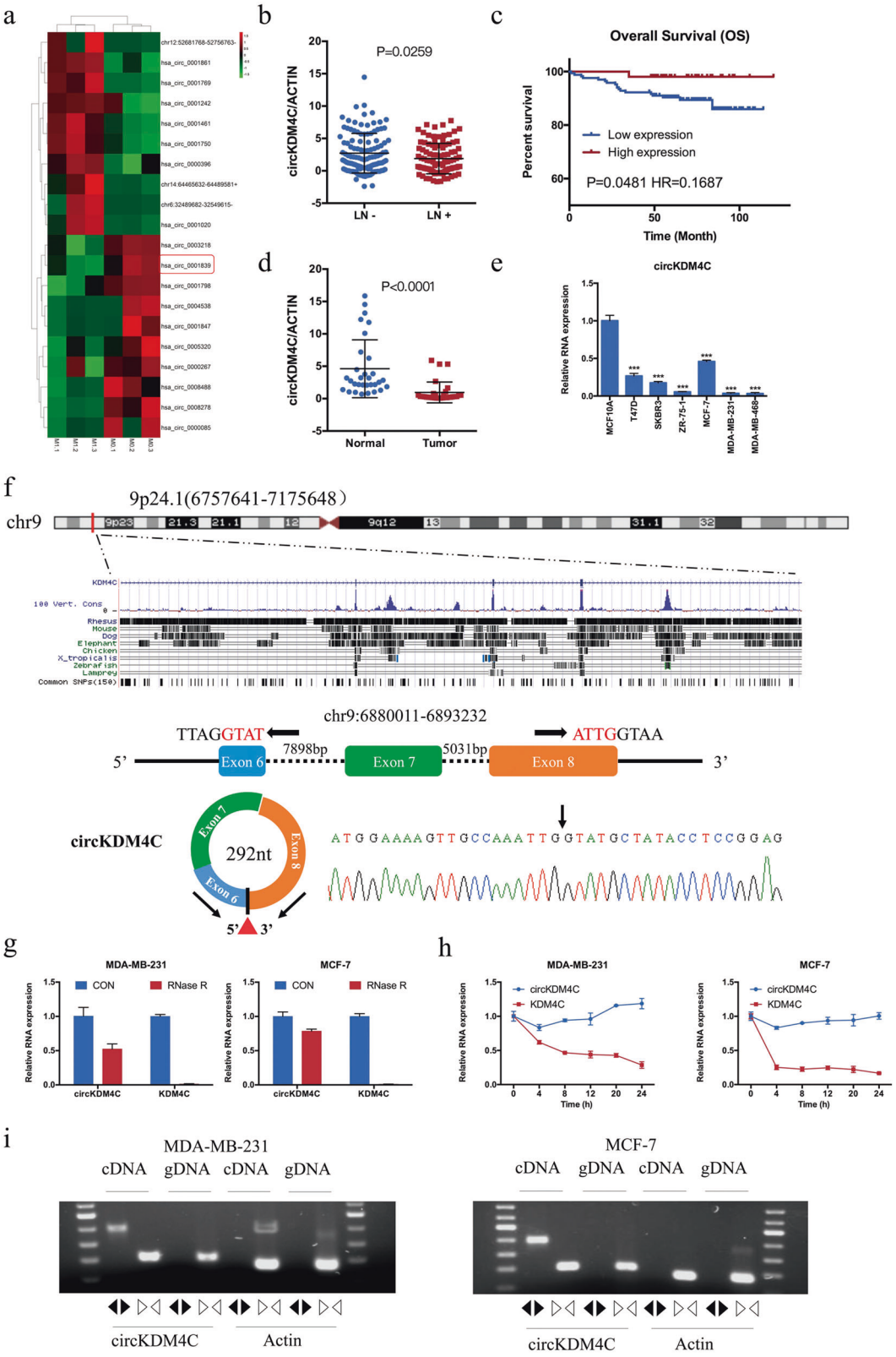

which is a typical epithelial phenotype, compared with the corresponding control cells (Fig. S1e). Furthermore, ectopic expression of circKDM4C inhibited cell growth, migration, and invasion, and promoted cell apoptosis (Fig. S2a–f). These findings collectively indicated that circKDM4C may inhibit the progression of breast cancer cells in vitro.

◀ **Fig. 1** CircKDM4C is downregulated in breast cancer and correlated with prognosis of breast cancer patients. **a** Hierarchical cluster analysis of microarray data was used to show the differential circRNA profiles in breast cancer with or without metastasis. Red and green denoted high and low expression, respectively. Each group was analyzed in triplicate. The expression of circKDM4C (has_circ_0001839) was indicated with a red rectangle. **b** The Expression of circKDM4C was decreased in breast cancer tissues with lymphatic metastasis. **c** Kaplan–Meier analysis revealed a positive association between circKDM4C expression and prognosis of breast cancer patients. **d** The expression of circKDM4C was decreased in breast cancer tissues compared with adjacent normal tissues. **e** qRT-PCR was used to examine the expression of circKDM4C in different breast cancer cells and normal breast cells. **f** The schematic diagram showed the genomic locus of circKDM4C in KDM4C gene. The expression of circKDM4C was validated by RT-PCR followed by sanger sequencing. Arrows represent divergent primers that bind to the genomic region of circKDM4C. **g** qRT-PCR analysis of circKDM4C and KDM4C RNA after treatment with RNase R in MDA-MB-231 and MCF-7 cells. **h** qRT-PCR analysis of circKDM4C and KDM4C RNA after treatment with Actinomycin D at the indicated time points in MDA-MB-231 and MCF-7 cells. **i** RT-PCR assay with divergent or convergent primers indicated the existence of circKDM4C in MDA-MB-231 and MCF-7 cells. Actin was used as a negative control. (***$p < 0.001$)

CircKDM4C inhibits the doxorubicin resistance of breast cancer cells in vitro

Given the relationship between high metastatic ability and enhanced chemoresistance, we further explored the effect of circKDM4C on doxorubicin resistance. Lower expression of circKDM4C was detected in doxorubicin-resistant cells compared with parental cells (Fig. 3a), indicating its inhibitory role in drug resistance. The IC_{50} value of doxorubicin was significantly higher in cells transfected with si-circKDM4C than in cells transfected with si-NC (Figs. 3b and S3a). We also found that doxorubicin led to cell growth inhibition in a time-dependent manner, and circKDM4C knockdown increased the resistance of breast cancer cells to doxorubicin (Figs. 3c and S3b). Consistently, MDA-MB-231/DOX cells transfected with the circKDM4C expression vector showed attenuated cell proliferation and decreased resistance to doxorubicin in a dose-dependent manner and a time-dependent manner (Fig. 3d–f). Colony formation assays revealed that circKDM4C knockdown promoted the colony-forming capacity of breast cancer cells (Fig. S3c). Moreover, cell proliferation was significantly higher in circKDM4C-downregulated cells compared with NC-transfected cells exposed to 0.4 μg/mL doxorubicin (Fig. S3c). Similarly, circKDM4C overexpression led to the inhibition of migration and invasion in doxorubicin-resistant cells (Fig. 3g). CircKDM4C knockdown suppressed doxorubicin-induced apoptosis, whereas circKDM4C overexpression led to enhanced apoptosis (Figs. 3h, i and S3d), as determined by flow cytometry and western blot assays. These results indicated that circKDM4C decreased the resistance to doxorubicin in breast cancer cells.

CircKDM4C acts as a miRNA sponge for miR-548p in breast cancer cells

Using nuclear/cytosol fractionation assay, we demonstrated that circKDM4C is predominately localized in the cytoplasm (Fig. 4a). According to the Circular RNA Interactome database, circKDM4C could act as a sponge for several miRNAs. The top-ranking potential binding sites of 11 miRNAs within the circKDM4C sequence are listed (Fig. 4b, Table S2). The Kaplan–Meier Plotter tool showed that high expression levels of miR-548p, miR-587, miR-610, miR-558, miR-1245a, miR-634, and miR-891b were associated with poor prognosis (Figs. 4c and S4a), indicating that these genes may play an oncogenic role in breast cancer. The expression of miR-548p was higher in breast cancer cells than in normal breast cells (Figs. 4d and S5a). CircKDM4C knockdown led to increased expression of these miRNAs (Figs. 4e and S5b), and increased expression of these miRNAs was found in MDA-MB-231/DOX cells (Figs. 4f and S5c). Among these changes, the change in miR-548p was the most significant, thus, we chose miR-548p as a potential target of circKDM4C. Luciferase assay revealed that miR-548p mimics significantly decreased the luciferase reporter activity of wild type but not mutant circKDM4C in a dose-dependent manner (Fig. 4g). In addition, the results of RIP assay showed that significantly more circKDM4C and miR-548p were pulled down with anti-AGO2 antibodies than with anti-IgG (Fig. 4h), suggesting an association between circKDM4C and miR-548p. Altogether, these results implied that circKDM4C might function as a ceRNA for miR-548p in breast cancer cells.

Overexpression of miR-548p promotes breast cancer progression and reverses the tumor suppressor role of circKDM4C in breast cancer cells

We then investigated the function of miR-548p in breast cancer cells. Increased expression of miR-548p significantly promoted the viability, migration, and invasion abilities of the cells (Fig. 4i–k). Moreover, miR-548p overexpression could promote DOX-resistance in breast cancer cells (Fig. 4l). Consistently, miR-548p mimics suppressed DOX-induced cell apoptosis as determined by flow cytometry (Figs. 4m and S5d). The rescue experiments showed that miR-548p mimics could partly abrogate the circKDM4C overexpression-mediated inhibition of proliferation, migration, invasion, and DOX-resistance in breast cancer cells (Fig. 5a–d). Above all, these data suggested that circKDM4C served as a tumor suppressor partly through abolishing the oncogenic effect of miR-548p in breast cancer cells.

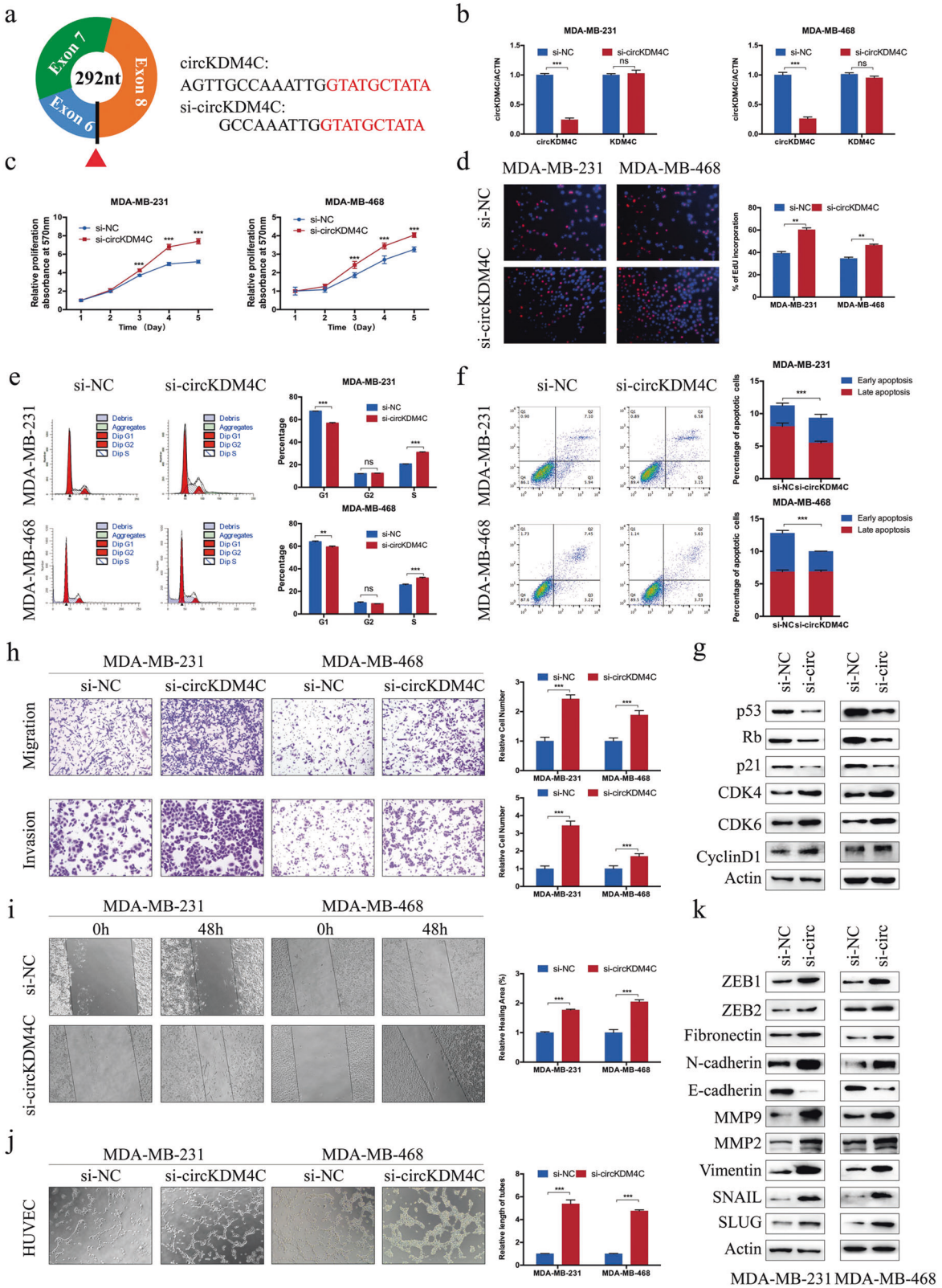
a
Exon 7
292nt
Exon 8
Exon 6
circKDM4C:
AGTTGCCAAATTGGTATGCTATA
si-circKDM4C:
GCCAAATTGGTATGCTATA
b
MDA-MB-231
MDA-MB-468
si-NC
si-circKDM4C
circKDM4C/ACTIN
circKDM4C
KDM4C
c
MDA-MB-231
MDA-MB-468
Relative proliferation absorbance at 570nm
Time (Day)
d
MDA-MB-231
MDA-MB-468
si-NC
si-circKDM4C
% of EdU incorporation
e
si-NC
si-circKDM4C
MDA-MB-231
MDA-MB-468
Debris
Aggregates
Dip G1
Dip G2
Dip S
Percentage
G1
G2
S
f
Early apoptosis
Late apoptosis
Percentage of apoptotic cells
g
si-NC
si-circ
p53
Rb
p21
CDK4
CDK6
CyclinD1
Actin
h
Migration
Invasion
Relative Cell Number
i
0h
48h
Relative Healing Area (%)
j
HUVEC
Relative length of tubes
k
ZEB1
ZEB2
Fibronectin
N-cadherin
E-cadherin
MMP9
MMP2
Vimentin
SNAIL
SLUG
Actin
MDA-MB-231 MDA-MB-468

◀ **Fig. 2** CircKDM4C knockdown promotes proliferation, migration, invasion, tube formation, and inhibits apoptosis of breast cancer cells. **a** Schematic illustration was used to show the target sequences of the siRNAs specific to the back-splicing junction of circKDM4C. **b** The interfering efficacies of circKDM4C-targeting siRNAs on circKDM4C and KDM4C mRNA were measured by qRT-PCR. MTT (**c**) and EdU (**d**) assays of MDA-MB-231 and MDA-MB-468 cells transfected with control or circKDM4C siRNAs were performed to evaluate cell proliferative ability. **e** Cell cycle distributions in circKDM4C knockdown cells were presented by flow cytometry. **f** Flow cytometry apoptosis analysis of MDA-MB-231 and MDA-MB-468 cells transfected with control or circKDM4C siRNAs. **g** Western blot was used to examine the expression of cell cycle-related proteins after circKDM4C knockdown. Si-circ was short for si-circKDM4C. **h** Cell migration and invasion abilities of MDA-MB-231 and MDA-MB-468 cells transfected with si-NC or si-circKDM4C were evaluated by the transwell assays. **i** Wound healing assay was performed to examine the migration abilities after circKDM4C knockdown. **j** The tube formation of HUVEC cells was promoted by treatment with the preconditioned medium of MDA-MB-231 and MDA-MB-468 cells transfected with circKDM4C siRNAs. **k** The overexpression of circKDM4C shifted the cell morphology from a mesenchymal to an endothelial phenotype. Cytoskeleton F-actin proteins were stained with FITC-phalloidin and viewed under a fluorescence microscope at 100× (upper panel) and 400× (lower panel) magnifications. Western blot indicated that circKDM4C was able to regulate the expression of EMT-related proteins. Si-circ was short for si-circKDM4C. (***$p < 0.001$; ns, no significance)

PBLD is downregulated in breast cancer tissues and regulated by circKDM4C as a miR-548p sponge

Through overlapping the results of miRNA target prediction by miRWalk, TargetScan, microT_CDS, mirDIP, and miRDB, the 3′-UTRs of 13 candidates were considered as putative targets of miR-548p (Fig. 6a, Table S3). We further analyzed the expression of these potential target genes in breast cancer tissues and their association with patient prognosis using TCGA and GEO databases. Among them, phenazine biosynthesis-like domain-containing protein (PBLD) expression was significantly lower in breast cancer tissues than in normal tissues (Fig. S6a). Moreover, high expression of PBLD was associated with better overall survival and disease free survival of breast cancer patients (Fig. S6b). Therefore, PBLD was selected as a putative target of miR-548p for further observation. MiR-548p mimics led to decreased fluorescence of the wild-type PBLD 3′-UTR, but had no effect on the mutant vectors (Fig. 6b). The mRNA and protein levels of PBLD were remarkably inhibited after miR-548p overexpression (Fig. 6c), in accordance with the circKDM4C knockdown results (Figs. 6c, d and S6c), indicating that circKDM4C could sponge miR-548p and modulate PBLD expression. The expression of PBLD in 35-matched tissues was examined, and PBLD was lower in breast cancer tissues compared with adjacent normal tissues (Fig. 6e). Moreover, the expression of PBLD was decreased in MDA-MB-231/DOX cells (Fig. 6f), indicating its suppressive role in doxorubicin resistance in breast cancer. PBLD knockdown significantly enhanced proliferation and doxorubicin resistance of breast cancer cells (Figs. 6g–i and S6d). The flow cytometry assays showed that PBLD knockdown promoted cell cycle progression as indicated that fewer cells were distributed in G1 phase (Fig. 6j); PBLD knockdown also suppressed cell apoptosis (Fig. 6k). Moreover, PBLD knockdown obviously promoted the migration and invasion of breast cancer cells (Fig. 6l). Collectively, these findings suggest that circKDM4C promotes breast cancer cell progression and doxorubicin resistance through protecting PBLD from miR-548p-mediated degradation.

CircKDM4C overexpression attenuates breast cancer progression and doxorubicin resistance in vivo

We further investigated the effects of increased circKDM4C expression on regulating tumor growth, doxorubicin resistance, and metastasis in vivo. The growth rates and tumor weights of the xenograft tumors were lower in the high circKDM4C expression group than in the control group (Fig. 7a–c). Moreover, the circKDM4C-overexpressing group treated with doxorubicin showed even greater reductions in tumor volumes and tumor weights (Fig. 7a–c). Consistently, circKDM4C overexpression significantly increased PBLD expression and led to decreased miR-548p expression; however, doxorubicin treatment resulted in the opposite trends (Fig. S7a). IHC analysis also showed that decreased ki67 and increased PBLD levels were identified in the circKDM4C-overexpressing groups (Figs. 7d and S7b). To establish a metastasis model, circKDM4C-overexpressing and control MDA-MB-231 cells were injected into BALB/c nude mice through tail veins. H&E staining was performed to pathologically confirm the metastatic nodules in the lungs (Fig. 7e). All five mice injected with control cells developed metastatic nodules with different sizes and quantities, whereas only two out of five mice in the circKDM4C-overexpressing group exhibited lung metastasis. Importantly, the volume and number of lung metastatic nodules were lower in the circKDM4C-overexpressing group than in the control group (Fig. 7e). Overall, these data indicated that increased circKDM4C expression efficiently suppressed growth, doxorubicin resistance, and metastasis of breast cancer in vivo.

Discussion

Many studies have shown that circRNAs are dysregulated in diverse cancer types, such as bladder cancer [21], gastric cancer [22], non-small cell lung cancer [23, 24], clear cell renal cell carcinoma [25], and hepatocellular carcinoma [26]. In the present study, we screened differentially expressed circRNAs in breast cancer tissues with or without

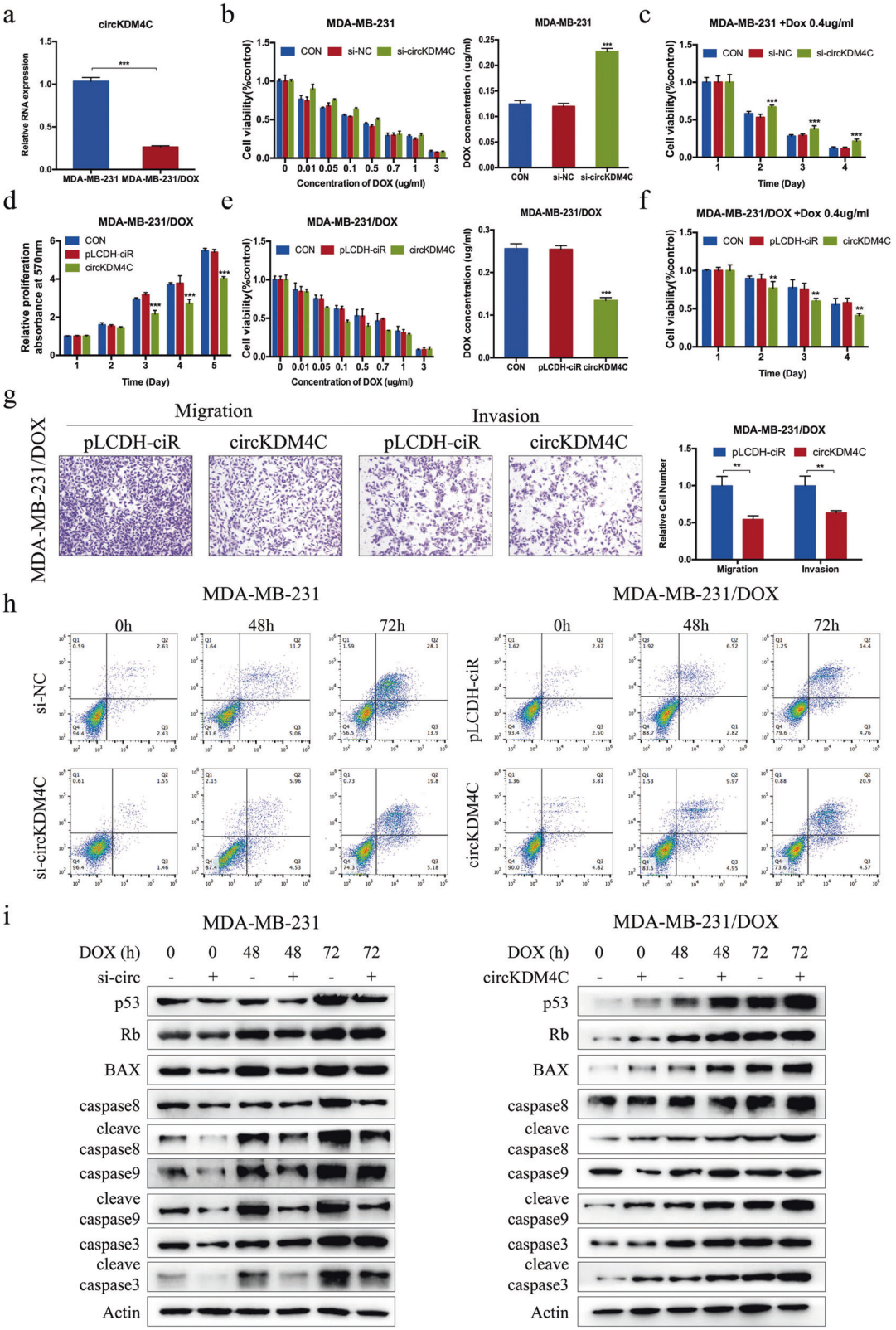

metastasis, and focused on the function and potential mechanism of decreased circKDM4C expression in breast cancer progression.

Given the abundance and stability of circRNAs, they are more suitable than other RNAs as potential cancer biomarkers. Previous studies have identified many circRNAs,

◀ **Fig. 3** CircKDM4C knockdown promotes resistance to doxorubicin of breast cancer cells. **a** The expression level of circKDM4C was significantly decreased in doxorubicin-resistant breast cancer cells compared with parental cells. **b** The IC_{50} value and viability of MDA-MB-231 cells in the si-circKDM4C group were increased compared with the control group. **c** Doxorubicin of 0.4 μg/ml was further used to test the promotion of drug resistance caused by circKDM4C knockdown in MDA-MB-231 cells. **d** MTT cell proliferation assays performed in MDA-MB-231/DOX cells transfected with circKDM4C expression vector or control vector. **e** The IC_{50} value and viability of MDA-MB-231/DOX cells in the circKDM4C-overexpressed group were decreased compared with the control groups. **f** Doxorubicin of 0.4 μg/ml was further used to test the inhibition of drug resistance caused by circKDM4C overexpression in MDA-MB-231/DOX cells. **g** Transwell assay was used to measure migration and invasion capacities in MDA-MB-231/DOX cells transfected with circKDM4C expression vector or control vector. **h** The cells were treated with 0.4 μg/ml doxorubicin for indicated time, then flow cytometry was used to examine the effect of circKDM4C on doxorubicin-induced apoptosis in MDA-MB-231 and MDA-MB-231/DOX cells. **i** Western blot showed the effect of circKDM4C and doxorubicin on the expression of apoptosis-related proteins (p53, RB, BAX, caspase-8, cleaved caspase-8, caspase-9, and cleaved caspase-9). (*$P < 0.05$, **$P < 0.01$, and ***$P < 0.001$)

such as circPVT1 [11], circTCF25 [27], and circHIPK3 [19], as cancer biomarkers in various cancers. Using a cohort of 219 breast cancer patients, we found that patients with low circKDM4C expression had a significantly shorter overall survival than those with high circKDM4C expression, and the expression of circKDM4C was correlated with lymphatic metastasis. Further studies showed that circKDM4C was capable of regulating breast cancer cell proliferation, metastasis, chemoresistance, and tumor growth both in vitro and in vivo, indicating its tumor-suppressive role in breast cancer. Recently, several studies revealed the significant role of circRNAs in the drug resistance of various cancers. Xiong et al. identified 71 differentially expressed circRNAs between chemoradiation-resistant colorectal cancer cells and parental cells, which regulate several cancer and cancer-related pathways, such as AKT and WNT signaling [28]. Trough comparing adriamycin (ADM) resistant MCF-7 breast cancer cells (MCF-7/ADM) and parental MCF-7 cells, 18 differentially expressed circRNAs were identified, and the circ-0006528/miR-7–5p/Raf1 axis was reported to play a role in breast cancer chemoresistance [29]. Moreover, circPVT1, a potential new biomarker for osteosarcoma patients, promoted resistance to doxorubicin and cisplatin in OS cells through reducing the expression of the classical drug resistance-related gene ABCB1 [30]. Doxorubicin is one of the most commonly used chemotherapeutics for breast cancer patients, however, the development of chemoresistance has limited its clinical application and little is known about the role of circRNAs in breast cancer chemoresistance. In this study, we identified that circKDM4C was downregulated in doxorubicin-resistant breast cancer cells. CircKDM4C knockdown or overexpression led to markedly increased or decreased doxorubicin resistance, respectively. Moreover, circKDM4C overexpression obviously inhibited the migration and invasion ability of doxorubicin-resistant breast cancer cells, further revealing the relationship between metastasis and chemoresistance [31, 32]. Cell apoptosis is one of the major effects of chemotherapeutics treatment on cancer cells [33], and circKDM4C could modulate the cells response to doxorubicin through regulating doxorubicin-induced apoptosis. CircKDM4C overexpression also improved the sensitivity of breast cancer cells to doxorubicin in vivo, indicating that circKDM4C may serve as a biomarker to predict the chemoresponse and prognosis of breast cancer patients.

Numerous studies have shown that circRNAs may regulate the expression of oncogenic or tumor-suppressive genes via acting as miRNA sponges [13]. For example, circITCH was able to suppress the Wnt/β-catenin pathway through inhibiting various miRNAs in different cancers [34–36]. CircHIPK3 was found to inhibit bladder cancer progression via sponging miR-558 [21], or served as an oncogene in colorectal cancer [19] and nasopharyngeal carcinoma [37] through sponging miR-7 or miR-4288. We found that circKDM4C was located mainly in the cytoplasm, which is thought to be a major characteristic of miRNA sponges [38]. Using bioinformatics algorithms, we predicted miR-548p as a potential target of circKDM4C, and further confirmed it by luciferase and RIP assays. Our data indicated that miR-548p overexpression significantly promoted breast cancer cell proliferation, migration, and invasion, and could partly abolish the circKDM4C-mediated biological effects and increased PBLD expression.

PBLD, also termed MAWBP, is widely expressed in human tissues, such as the liver, kidney, and stomach. Using proteomic strategies, PBLD was first found to be downregulated in gastric cancer tissues and to have a high affinity for MAWD [39]. Further study revealed that PBLD negatively regulated gastric cancer cell growth and migration in vitro and in vivo, and inhibited TGF-β1-induced EMT through suppressing the phosphorylation and nuclear translocation of p-Smad3 [40]. Moreover, the expression of PBLD was also closely associated with the gastric cancer differentiation grade through mediating the expression of differentiation-related proteins, such as E-cadherin, pepsinogen C, N-cadherin, and Snail, through TGF-β signaling [41]. In addition, PBLD has been proven to be significantly downregulated in hepatocellular carcinoma tissues, and low PBLD expression was associated with a poor prognosis in HCC patients [42]. Using microarray analysis, the attenuated hepatocellular carcinoma cell growth and metastasis caused by PBLD overexpression was associated with the inhibition of various tumor progression-related signaling pathways, such as VEGF-A, MAPK, NF-κB, EMT, angiogenesis, and others [43]. Until now, however, there has been a lack of studies focusing on PBLD expression and function in breast cancer. We confirmed that the expression of PBLD was decreased in breast cancer

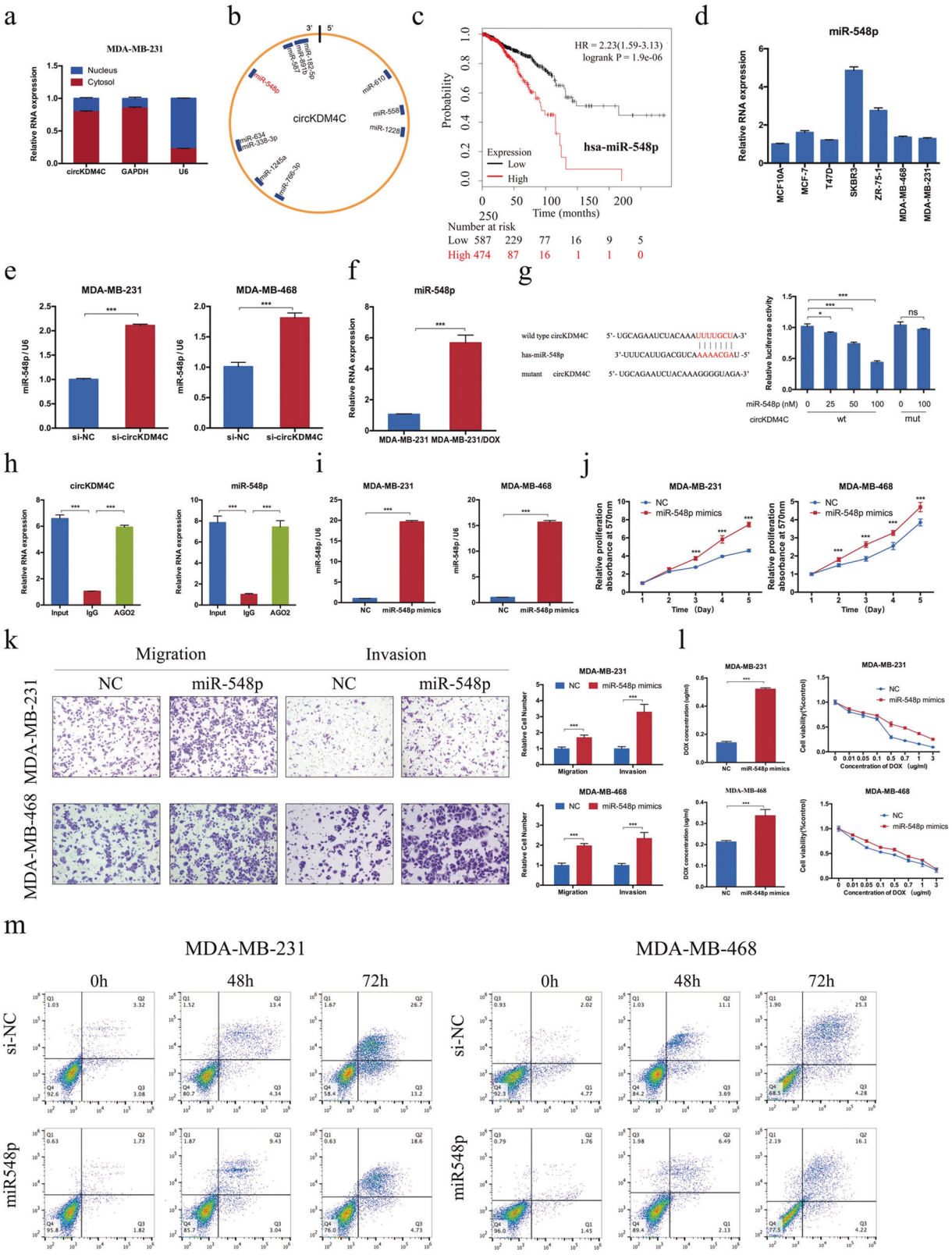

tissues and that PBLD knockdown led to enhanced progression and chemoresistance in breast cancer. Moreover, circKDM4C promoted breast cancer progression by promoting PBLD expression through interacting with miR-548p. Hence, we provided further evidence for the posttranscriptional regulation of PBLD by a circRNA in breast cancer.

◀ **Fig. 4** CircKDM4C serves as a sponge of miR-548p and miR-548p promotes proliferation, migration, and invasion of breast cancer cells. **a** qRT-PCR analysis of circKDM4C nuclear and cytoplasmic expression levels in MDA-MB-231 cells. U6 was used as a nucleus marker, and GAPDH was used as a cytosol marker. **b** A schematic model showing the putative-binding sites for miRNAs and circKDM4C. **c** Kaplan–Meier analysis revealed that high expression of miR-548p was correlated with poor prognosis of breast cancer patients. **d** The expression of miR-548p in different breast cancer cells and normal breast cells was analyzed by qRT-PCR. **e** Knockdown of circKDM4C led to increased expression of miR-548p. **f** The expression of miR-548p was increased in MDA-MB-231/DOX cells compared with parental cells. **g** Schematic illustration showed the predicted binding sites between circKDM4C and miR-548p, and mutation of potential miR-548p-binding sequence in circKDM4C (upper). Luciferase assays were performed in HEK293T cells transfected with luciferase reporter containing circKDM4C sequence with wild-type or mutant miR-548p-binding sites and the mimics of miR-548p or control (lower). **h** RIP experiments were performed in HEK293T cells, and the expression of miR-548p and circKDM4C in the AGO2 coprecipitation was detected by qRT-PCR. **i** The efficiency of miR-548p overexpression was determined by qRT-PCR. **j** MTT assays indicated the increased proliferative ability in breast cancer cells transfected with miR-548p mimics. **k** The migration and invasion capabilities of breast cancer cells were promoted by miR-5480 overexpression. **l** Overexpression of miR-548p led to increased resistance to doxorubicin of breast cancer cells. **m** The cells were treated with 0.4 μg/ml doxorubicin for indicated time, then the flow cytometry assay showed that miR-548p overexpression attenuated doxorubicin-induced apoptosis in breast cancer cells. (*$P < 0.05$, **$P < 0.01$, and ***$P < 0.001$)

In summary, we demonstrated for the first time that circKDM4C was downregulated in breast cancer tissues and cell lines. Our results not only elucidate the potential mechanism by which circRNAs regulate the progression and chemoresistance of breast cancer, but also suggest that the circKDM4C/miR-548p/ PBLD axis could be a potential therapeutic target for breast cancer patients.

Materials and methods

Patients and specimens

The breast cancer tissues tumor and normal tissues were obtained from patients who were diagnosed with breast cancer and undergone surgery from February 2009 to January 2015 in Qilu Hospital of Shandong University. The median follow-up is 69 months. Tissue samples were stored at −80 °C until RNA extraction. Informed consent for the use of these clinical materials in research was obtained. All experimental procedures were approved by the Ethical Committee of Shandong University.

Microarray analysis

Total RNA from three breast cancer tissues with or without metastasis was used for Arraystar Human circRNA Array according to the standard protocols. Briefly, total RNAs were digested with RNase R to eliminate linear RNAs, and the enrich circRNAs were used to construct RNA libraries. Then, the denatured single-stranded DNA molecules were captured, amplified in situ as clusters and finally sequenced on Illumina HiSeq Sequencer When the circRNA expression level changed at least 1.5-fold with $p < 0.05$, the circRNA expression was considered to be differentially expressed.

Cell culture and cell transfection

All the cell lines were purchased from American Type Culture Collection (ATCC, USA). The cell lines were characterized by Genetic Testing Biotechnology Corporation (Suzhou, China) using short tandem repeat markers and tested for negative mycoplasma contamination using Mycoplasma Detection Kit (Sigma). Cells were routinely cultured in Dulbecco's modified Eagle's medium (Invitrogen, Carlsbad, CA, USA) containing 10% fetal bovine serum (FBS) (Hyclone), 100 U/ml penicillin, and 100 μg/ml streptomycin in a humidified atmosphere containing 5% CO2 at 37 °C. Lipofectamine 2000 regent (Invitrogen, MA, USA) was used for cell transfection.

The sequences of exon 6, 7, and 8 of KDM4C with a length of 292 bp were cloned into a pLCDH-ciR-vector (Invitrogen, Carlsbad, CA, USA) to generate pLCDH-circKDM4C constructs. The pLCDH-ciR empty vector was used as negative control and the primers used for vector construction was showed in Table S4. The transfected cells were screened with puromycin (2 μg/ml) for 4 weeks to establish circKDM4C overexpression and control cell lines. PBLD knockdown cell lines were transfected with PBLD or shPBLD. All the mimics and siRNAs were purchased from Applied Biological Materials (ABM, Canada).

RNA extraction and qRT-PCR

Total RNA was isolated from tissues or cells using Trizol reagant (Invitrogen, USA). Then cDNA was synthesized using PrimeScript reverse transcriptase (RT) reagent kit (TaKaRa, Shiga, Japan). qRT-PCR was carried out using the SYBR green PCR mix (Takara). Actin and U6 were used as the endogenous control for mRNA or microRNAs, respectively. The primers were listed in Table S4.

Actinomycin D and RNase R treatment

Transcription was prevented by the addition of 2 μg/ml actinomycin D (Sigma-Aldrich, USA) or DMSO (Mock) (Sigma-Aldrich, USA) as the negative control for indicated

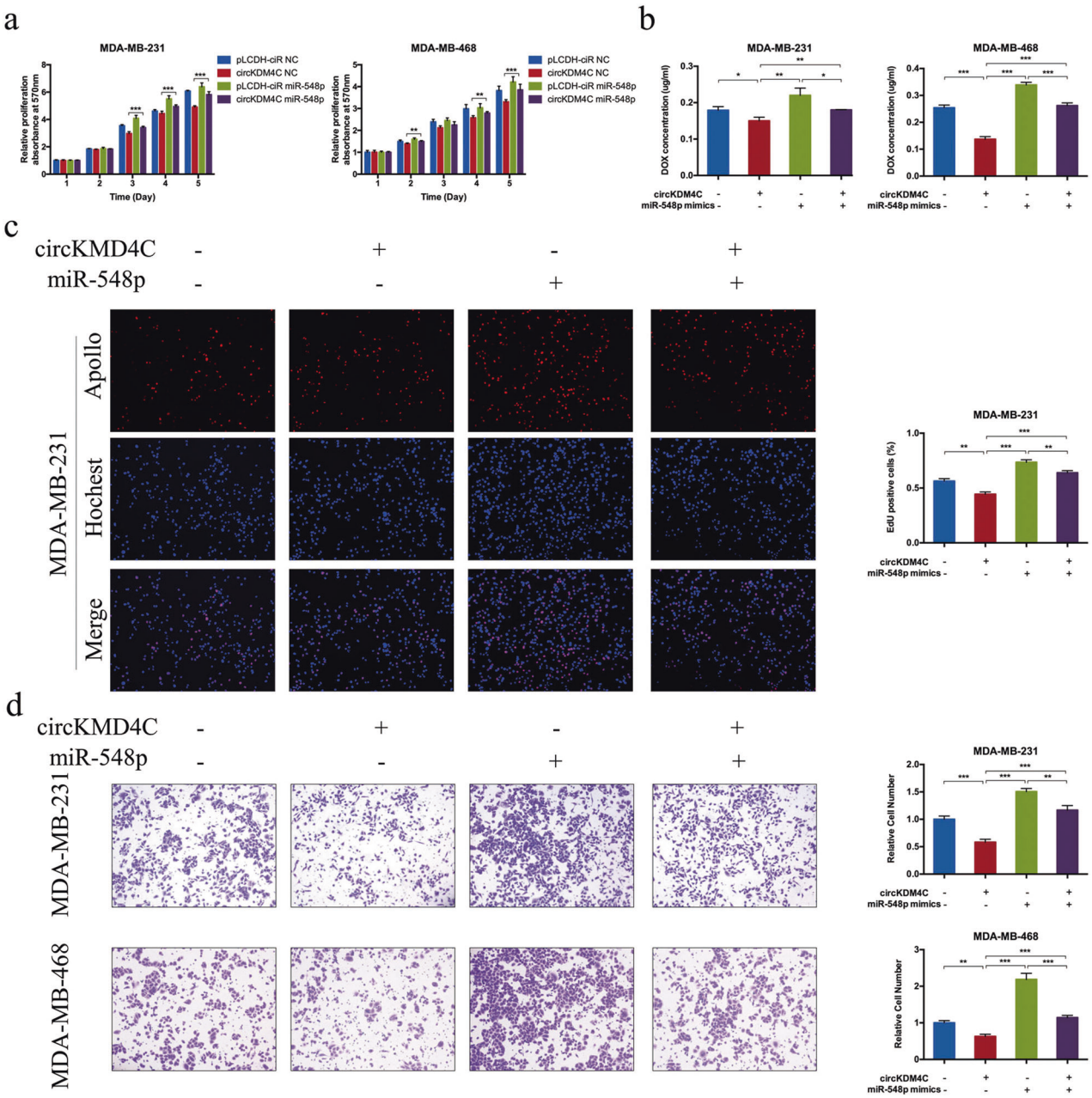

Fig. 5 Overexpression of miR-548p effectively reverses circKDM4C-induced inhibition of cell progression and doxorubicin resistance. **a**–**d** MDA-MB-231 and MDA-MB-468 cells transfected with miR-NC, miR-548p, pLCDH-ciR, or circKDM4C alone or simultaneously. Then the ability of cell proliferation, resistance to doxorubicin, migration, and invasion was, respectively, assessed by MTT (**a**), IC_{50} analysis (**b**), EdU assay (**c**), and the transwell migration and matrigel invasion (**d**) assay. (*$P < 0.05$, **$P < 0.01$, and ***$P < 0.001$)

time. RNase R treatment is used to identify and confirm the character of circRNA. The RNAs extracted from MDA-MB-231 or MCF-7 cells were divided into two equal parts respectively, one for RNase R treatment (RNase R) and the other for nontreatment (Mock). Total RNA (2 μg) was incubated for 30 min at 37 °C with 3 U/μg of RNase R. After treatment with actinomycin D and RNase R, the RNA expression levels of circKDM4C and KDM4C were detected by qRT-PCR. The internal reference (actin) in the mock group is used as the calculation standard [44].

Cell proliferation assay and in vitro chemosensitivity assay

The transfected cells were seeded into 96-well plates at a density of 1500 cells per well. After incubation overnight,

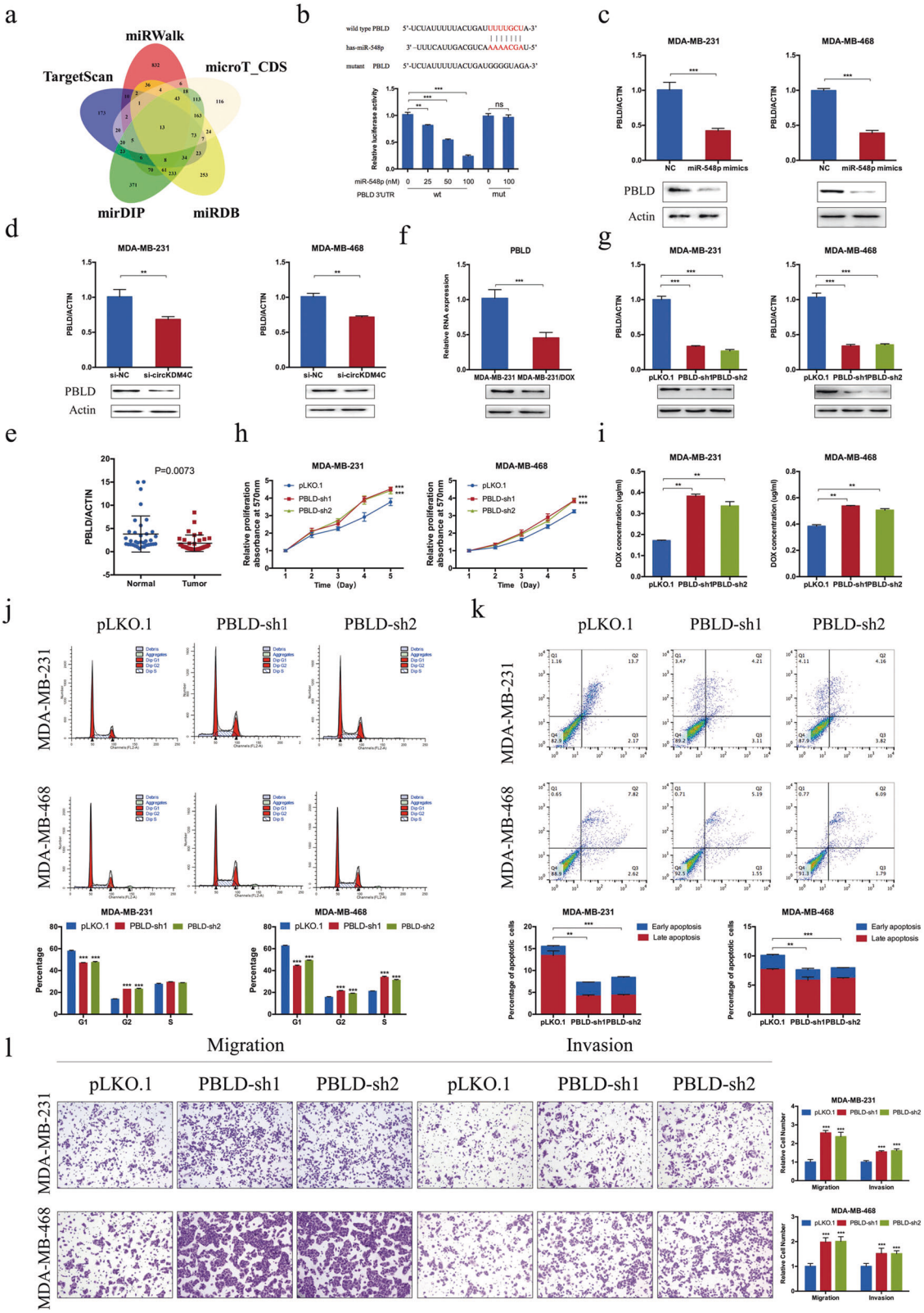

the medium was replaced by the solutions containing indicated concentrations of doxorubicin for the indicated time. Then 20 µl of MTT (5 mg/ml) was added into the wells and incubated for another 4 h. The supernatants were aspirated and 100 µl of DMSO was add into the wells. The absorbance values were measured using a

◀ **Fig. 6** CircKDM4C inhibited breast cancer cell progression and doxorubicin resistance through protecting PBLD from miR-548p-induced degradation. **a** Schematic illustration showing the overlapping of the target genes of miR-548p predicted by TargetScan, miRWalk, mirDIP, miRDB, and microT_CDS. **b** Schematic illustration and luciferase assay were used to show the regulatory relationship between miR-548p and PBLD. **c** Overexpression of miR-548p in MDA-MB-231 and MDA-MB-468 cells led to decreased PBLD mRNA (upper histograms) and protein (lower bands) levels. **d** Knockdown of circKDM4C caused reduced PBLD mRNA (upper histograms) and protein (lower bands) expression. **e** The expression of PBLD was downregulated in breast cancer tissues compared with adjacent normal tissues. **f** The mRNA (upper histogram) and protein (lower bands) expression of PBLD was decreased in cells with higher resistance to doxorubicin or higher metastatic potential. **g** The knockdown efficiency of shPBLD vectors was examined by qRT-PCR (upper histograms) and western blot (lower bands). PBLD knockdown led to decreased proliferation ability (**h**) and resistance to doxorubicin (**i**) of breast cancer cells. **j** Flow cytometry assay was used to evaluate the effect of PBLD knockdown on cell cycle. **k** PBLD knockdown led to attenuated cell apoptosis. **l** Transwell assays revealed that PBLD knockdown promoted migration and invasion abilities of breast cancer cells. (**$P < 0.01$, and ***$P < 0.001$)

Microplate Reader (Bio-Rad, Hercules, CA, USA) at 570 nm.

Establishment of doxorubicin-resistant cells

The doxorubicin-resistant breast cancer cells (MDA-MB-231/DOX) were generated from the parental MDA-MB-231 cells by continuous exposure to increasing concentrations of doxorubicin (Sigma, USA), starting from 0.01 μg/ml and terminating with 1 μg/ml over a period of 6 months. To maintain the DOX-resistant phenotype, MDA-MB-231/DOX cells were incubated with the culture medium containing 0.01 μg/ mL DOX.

Colony formation assay

The transfected cells were seeded into six-well plates at a density of 500 cells per well with or without 0.4 μg/ml doxorubicin. After 2 weeks, the cells were washed with cold PBS twice, fixed with methanol, and stained with 0.1% crystal violet solution. Pictures were imaged and counted.

EdU incorporation assay

The EdU Proliferation Kit (RiboBio Guangzhou, China) was used to assess cell proliferation viability. Briefly, 48 h after transfection, 1×10^4 cells were seeded in 96-well plate. After incubation with 50 mM EdU for 2.5 h, the cells were fixed with 4% paraformaldehyde (PFA) and stained with Apollo Dye Solution. Hoechst was used to stain the nucleic acid. Images were obtained with an Olympus microscope (Olympus, Tokyo, Japan).

Cell cycle and apoptosis assays

For the cell cycle analysis, the transfected cells were stained with propidium iodide (PI) in the dark for 30 min, cell cycle distribution was measured by flow cytometry (Becton Dickinson, NJ, USA). Annexin V Apoptosis Detection Kit (BD Biosciences, NJ, USA) was used to detect cell apoptosis. Cells were collected and washed with ice cold PBS, followed by stained with 5 μL Annexin V-FITC and 5 μL PI, and incubated in the dark for 15 min. The ratio of apoptotic cells was obtained by flow cytometry and data were analyzed by FlowJo software.

Protein isolation and western blot

Cells were lysed with RIPA buffer and PMSF (Biocolors, Shanghai, China), separated by 10% SDS-PAGE, and electro-blotted onto a PVDF membrane (Millipore). After blocking with 5% nonfat milk, the membrane was incubated with various specific primary antibodies overnight at 4 °C. Blots were washed and incubated with horseradish peroxydase-coupled secondary antibodies (Millipore) for 2 h. The protein bands were detected using the Pro-lighting HRP agent. Expression of β-actin was used as a loading control. The primary antibodies and secondary antibodies used were available in Table S5.

Transwell migration and matrigel invasion assays

For migration assay, 1×10^5 of transfected cells suspended in the serum-free medium with Mitomycin C (5 μg/ml, sigma) were added into the upper wells, while the lower wells were filled with medium containing 20% FBS. After incubation for 24–48 h, the infiltrating cells were fixed with methanol and stained with 0.1% crystal violet. The invasion assay was performed in the same way as the migration assay except that the membrane was coated with matrigel. The cells on the lower surface were photographed and counted by ImageJ software.

Wound healing assay

Cells were seeded in a 24-well plate and incubated in DMEM containing 10% FBS until a confluent monolayer had formed. Then a sterile 200 μl plastic pipette tip was used to make scratches on the single cell layer and PBS was used to remove the detached cells. Cells were grown in serum-free DMEM and Mitomycin C (5 μg/ml, sigma) to inhibit cell proliferation, and images were captured at the

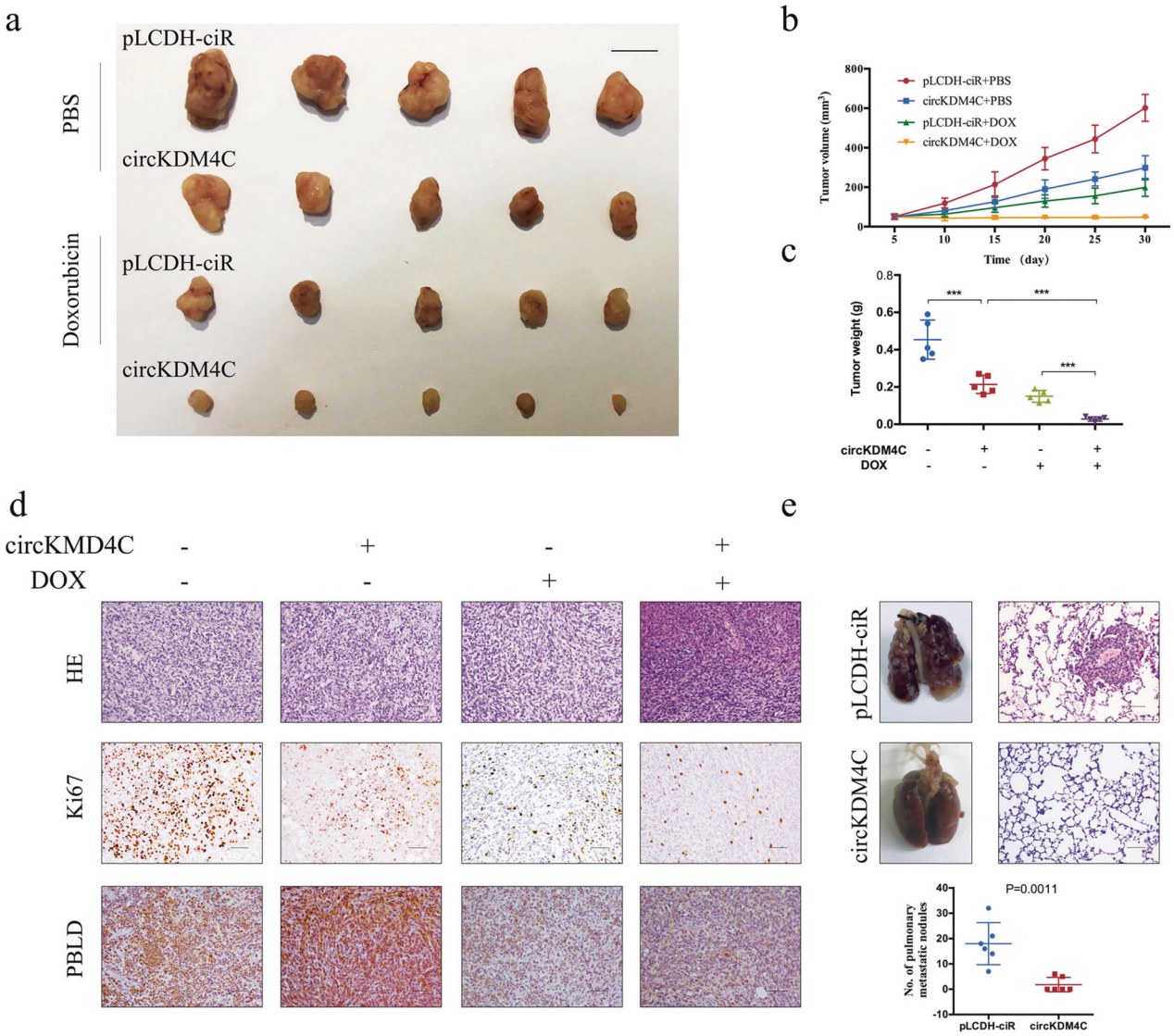

Fig. 7 Enforced expression of circKDM4C suppresses the growth, doxorubicin resistance, and metastasis of breast cancer cells in vivo. MDA-MB-231 cells were stably transfected with circKDM4C expression vector or pLCDH-ciR vector and injected subcutaneously into nude mice. When the average tumor size reached ~50 mm^3, doxorubicin was administered through intraperitoneal injection at a dose of 1 mg/kg every five day for a total of five doses. **a** Photographs illustrated tumors in xenografts. Scare bar = 1 cm. **b** Growth curve of xenograft tumors after the first administration of doxorubicin. **c** CircKDM4C overexpression or doxorubicin treatment significantly decreased the tumor weight. **d** H&E staining showed the tissue morphology and IHC staining analysis revealed of decreased expression of proliferation index Ki67 and PBLD. Scare bar = 50 μm. **e** Representative images of lung metastatic nodules and H&E staining of lungs isolated from mice injected with circKDM4C or control vectors transfected cells ($n = 5$ for each group). The corresponding statistical plots were presented in lower panel. Scare bar = 50 μm. (***$P < 0.001$)

indicated times (0 and 48 h) using an Olympus light microscope.

Tube formation assay

Transfected breast cancer cells were incubated for 48 h, and then the medium was collected. After being centrifuged at 500 g to remove detached cells and centrifuged at 12000 × g to discard cell debris, the condition medium (CM) was used for subsequent coculture experiments.

HUVECs were seeded in 48-well plates (1×10^5 cells/well) precoated with growth Matrigel (BD Biosciences, NJ, USA), and then cultured in the indicated condition medium. After 4–6 h of incubation, the formation of the tube network was imaged and quantified using an inverted microscope.

Morphological analysis

circKDM4C-overexpressed MDA-MB-231 cells were fixed with 4% PFA for 30 min and permeabilized with 0.1%

Triton X-100 for 3 min at room temperature. Then cells were stained for 60 min with 5 μg/ml of FITC-phalloidin (Sigma, USA) and stained with DAPI for 15 min. After rigorous washing, cultured cells on slips were viewed under a fluorescence microscope.

RNA immunoprecipitation (RIP)

RIP assay was carried out by using a Magna RIP™ RNA-Binding Protein Immunoprecipitation Kit (Millipore, Billerica, MA) according to the manufacturer's instructions. Human anti-AGO2 antibody or negative control mouse IgG (Millipore, Billerica, MA, USA) were used for RNA immunoprecipitation assay. Extracted RNAs were analyzed by qRT-PCR to detect the presence of circKDM4C and miR-548p.

Luciferase reporter assay

Cells were cotransfected with pmirGLO plasmids containing wild or mutant circKDM4C or PBLD 3′UTR and miRNA mimics using Lipofectamine 2000 (Invitrogen). After 48 h, luciferase activities were determined by the Dual-Luciferase Reporter Assay Kit (Promega). Results are presented as ratios of luminescence from firefly to Renilla luciferase.

In vivo tumorigenesis and metastasis assay

Female BALB/c nude mice (4 weeks old) were randomly divided into two groups, with ten mice in each group. MDA-MB-231 cells stably transfected with circKDM4C overexpression plasmids or control vectors were injected subcutaneously into the upper back of mice (3×10^6, 200 μl) randomly. When the tumor volumes reached about 50 mm^3, mice in each group were randomly divided into two groups, with five mice in each group. Then 1 mg/kg doxorubicin or PBS was injected via the tail vein every 5 days. No blinding was performed for the animal experiments. Tumor growth was calculated by measuring the length (L) and width (W) of the tumor every 5 days with a caliper. Tumor volume was calculated as $1/2LW^2$. After 30 days, the mice were killed, and the tumors were dissected and weighed. For metastasis assay, 5×10^5 breast cancer cells were injected into the tail veins of 4–5-week-old BALB/c nu/nu female mice randomly. After 4 weeks, all the mice were killed under anesthesia. The lungs were collected and fixed in 10% formalin. For tissue morphology evaluation, hematoxylin and eosin (HE) staining was performed. All procedures were approved and conducted in conformity to the guidelines for animal experiments by Shandong University Animal Care and Use Committee.

Immunohistochemistry (IHC)

Tumor tissues were fixed and cut into 4 μm sections. The slides were treated for antigen retrieval and incubated with primary antibodies (PBLD, 1:200, Ki67, 1:200) overnight at 4 °C, following by peroxidase-conjugated secondary antibody for 2 h at room temperature. Then the tissue sections were stained with diaminobenzidine, and counterstained with hematoxylin. Olympus light microscope was used to take photos for the representative areas.

Statistical analysis

The student's *t*-test was performed to analyze whether two experimental groups have significant difference. The data in statistical tests are conformed to normal distribution and the variance are similar. A two-tailed value of $P < 0.05$ was considered statistically significant. Data are expressed as mean ± S.D. from at least three independent experiments. Survival analysis was performed by Kaplan–Meier curves and log-rank test for significance.

Acknowledgements This work was supported by the National Natural Science Foundation of China (No. 81272903; No. 81672613; No. 81502285; No. 81602329), China Postdoctoral Science Foundation to NZ (2018M630787), the Key Research and Development Program of Shandong Province (No. 2015GSF118093, No. 2016GSF201119), the Natural Science Foundation of Shandong Province (ZR2014HQ078), the Shandong Science and Technology Development Plan (2016CYJS01A02), and the Special Support Plan for National High Level Talents ("Ten Thousand Talents Program") to QY.

Compliance with ethical standards

Conflict of interest The authors declare that they have no conflict of interest.

References

1. Bray F, Ferlay J, Soerjomataram I, Siegel RL, Torre LA, Jemal A. Global cancer statistics 2018: GLOBOCAN estimates of incidence and mortality worldwide for 36 cancers in 185 countries. CA: a cancer journal for clinicians; 2018.
2. Jones SE. Metastatic breast cancer: the treatment challenge. Clin breast cancer. 2008;8:224–33.
3. Maishman T, Cutress RI, Hernandez A, Gerty S, Copson ER, Durcan L, et al. Local recurrence and breast oncological surgery in young women with breast cancer: the POSH observational cohort study. Ann Surg. 2017;266:165–72.
4. O'Reilly EA, Gubbins L, Sharma S, Tully R, Guang MH, Weiner-Gorzel K, et al. The fate of chemoresistance in triple negative breast cancer (TNBC). BBA Clin. 2015;3:257–75.
5. Kim C, Gao R, Sei E, Brandt R, Hartman J, Hatschek T, et al. Chemoresistance evolution in triple-negative breast cancer delineated by single-cell sequencing. Cell. 2018;173:879–93 e13.

6. Cocquerelle C, Mascrez B, Hetuin D, Bailleul B. Mis-splicing yields circular RNA molecules. FASEB J. 1993;7:155–60.
7. Barrett SP, Wang PL, Salzman J. Circular RNA biogenesis can proceed through an exon-containing lariat precursor. eLife. 2015;4:e07540.
8. Chen LL, Yang L. Regulation of circRNA biogenesis. RNA Biol. 2015;12:381–8.
9. Salzman J, Gawad C, Wang PL, Lacayo N, Brown PO. Circular RNAs are the predominant transcript isoform from hundreds of human genes in diverse cell types. PLoS ONE. 2012;7:e30733.
10. Jeck WR, Sorrentino JA, Wang K, Slevin MK, Burd CE, Liu J, et al. Circular RNAs are abundant, conserved, and associated with ALU repeats. RNA. 2013;19:141–57.
11. Chen J, Li Y, Zheng Q, Bao C, He J, Chen B, et al. Circular RNA profile identifies circPVT1 as a proliferative factor and prognostic marker in gastric cancer. Cancer Lett. 2017;388:208–19.
12. Wei X, Li H, Yang J, Hao D, Dong D, Huang Y, et al. Circular RNA profiling reveals an abundant circLMO7 that regulates myoblasts differentiation and survival by sponging miR-378a-3p. Cell death Dis. 2017;8:e3153.
13. Hansen TB, Jensen TI, Clausen BH, Bramsen JB, Finsen B, Damgaard CK, et al. Natural RNA circles function as efficient microRNA sponges. Nature. 2013;495:384–8.
14. Du WW, Yang W, Liu E, Yang Z, Dhaliwal P, Yang BB. Foxo3 circular RNA retards cell cycle progression via forming ternary complexes with p21 and CDK2. Nucleic acids Res. 2016;44:2846–58.
15. Sang M, Meng L, Sang Y, Liu S, Ding P, Ju Y, et al. Circular RNA ciRS-7 accelerates ESCC progression through acting as a miR-876-5p sponge to enhance MAGE-A family expression. Cancer Lett. 2018;426:37–46.
16. Shi Z, Chen T, Yao Q, Zheng L, Zhang Z, Wang J, et al. The circular RNA ciRS-7 promotes APP and BACE1 degradation in an NF-kappaB-dependent manner. FEBS J. 2017;284:1096–109.
17. Li RC, Ke S, Meng FK, Lu J, Zou XJ, He ZG, et al. CiRS-7 promotes growth and metastasis of esophageal squamous cell carcinoma via regulation of miR-7/HOXB13. Cell death Dis. 2018;9:838.
18. Zheng Q, Bao C, Guo W, Li S, Chen J, Chen B, et al. Circular RNA profiling reveals an abundant circHIPK3 that regulates cell growth by sponging multiple miRNAs. Nat Commun. 2016;7:11215.
19. Zeng K, Chen X, Xu M, Liu X, Hu X, Xu T, et al. CircHIPK3 promotes colorectal cancer growth and metastasis by sponging miR-7. Cell death Dis. 2018;9:417.
20. Chen G, Shi Y, Liu M, Sun J. circHIPK3 regulates cell proliferation and migration by sponging miR-124 and regulating AQP3 expression in hepatocellular carcinoma. Cell death Dis. 2018;9:175.
21. Li Y, Zheng F, Xiao X, Xie F, Tao D, Huang C, et al. CircHIPK3 sponges miR-558 to suppress heparanase expression in bladder cancer cells. EMBO Rep. 2017;18:1646–59.
22. Zhang J, Liu H, Hou L, Wang G, Zhang R, Huang Y, et al. Circular RNA_LARP4 inhibits cell proliferation and invasion of gastric cancer by sponging miR-424-5p and regulating LATS1 expression. Mol cancer. 2017;16:151.
23. Wang L, Tong X, Zhou Z, Wang S, Lei Z, Zhang T, et al. Circular RNA hsa_circ_0008305 (circPTK2) inhibits TGF-beta-induced epithelial-mesenchymal transition and metastasis by controlling TIF1gamma in non-small cell lung cancer. Mol cancer. 2018;17:140.
24. Tan S, Sun D, Pu W, Gou Q, Guo C, Gong Y, et al. Circular RNA F-circEA-2a derived from EML4-ALK fusion gene promotes cell migration and invasion in non-small cell lung cancer. Mol cancer. 2018;17:138.
25. Wang K, Sun Y, Tao W, Fei X, Chang C. Androgen receptor (AR) promotes clear cell renal cell carcinoma (ccRCC) migration and invasion via altering the circHIAT1/miR-195-5p/29a-3p/29c-3p/CDC42 signals. Cancer Lett. 2017;394:1–12.
26. Shi L, Yan P, Liang Y, Sun Y, Shen J, Zhou S, et al. Circular RNA expression is suppressed by androgen receptor (AR)-regulated adenosine deaminase that acts on RNA (ADAR1) in human hepatocellular carcinoma. Cell Death Dis. 2017;8:e3171.
27. Zhong Z, Lv M, Chen J. Screening differential circular RNA expression profiles reveals the regulatory role of circTCF25-miR-103a-3p/miR-107-CDK6 pathway in bladder carcinoma. Sci Rep. 2016;6:30919.
28. Xiong W, Ai YQ, Li YF, Ye Q, Chen ZT, Qin JY, et al. Microarray analysis of circular RNA expression profile associated with 5-Fluorouracil-based chemoradiation resistance in colorectal cancer cells. BioMed Res Int. 2017;2017:8421614.
29. Gao D, Zhang X, Liu B, Meng D, Fang K, Guo Z, et al. Screening circular RNA related to chemotherapeutic resistance in breast cancer. Epigenomics. 2017;9:1175–88.
30. Kun-Peng Z, Xiao-Long M, Chun-Lin Z. Overexpressed circPVT1, a potential new circular RNA biomarker, contributes to doxorubicin and cisplatin resistance of osteosarcoma cells by regulating ABCB1. Int J Biol Sci. 2018;14:321–30.
31. Cai J, Fang L, Huang Y, Li R, Xu X, Hu Z, et al. Simultaneous overactivation of Wnt/beta-catenin and TGFbeta signalling by miR-128-3p confers chemoresistance-associated metastasis in NSCLC. Nat Commun. 2017;8:15870.
32. Xu H, Lin F, Wang Z, Yang L, Meng J, Ou Z, et al. CXCR2 promotes breast cancer metastasis and chemoresistance via suppression of AKT1 and activation of COX2. Cancer Lett. 2018;412:69–80.
33. Wang Y, Zhang L, Zheng X, Zhong W, Tian X, Yin B, et al. Long non-coding RNA LINC00161 sensitises osteosarcoma cells to cisplatin-induced apoptosis by regulating the miR-645-IFIT2 axis. Cancer Lett. 2016;382:137–46.
34. Li F, Zhang L, Li W, Deng J, Zheng J, An M. et al. Circular RNA ITCH has inhibitory effect on ESCC by suppressing the Wnt/beta-catenin pathway. Oncotarget. 2015;6:6001–13.
35. Wan L, Zhang L, Fan K, Cheng ZX, Sun QC, Wang JJ. Circular RNA-ITCH suppresses lung cancer proliferation via inhibiting the Wnt/beta-catenin pathway. BioMed Res Int. 2016;2016:1579490.
36. Huang G, Zhu H, Shi Y, Wu W, Cai H, Chen X. cir-ITCH plays an inhibitory role in colorectal cancer by regulating the Wnt/beta-catenin pathway. PLoS ONE. 2015;10:e0131225.
37. Ke Z, Xie F, Zheng C, Chen D. CircHIPK3 promotes proliferation and invasion in nasopharyngeal carcinoma by abrogating miR-4288-induced ELF3 inhibition. J Cell Physiol. 2019;234:1699–1706.
38. Xie F, Li Y, Wang M, Huang C, Tao D, Zheng F, et al. Circular RNA BCRC-3 suppresses bladder cancer proliferation through miR-182-5p/p27 axis. Mol cancer. 2018;17:144.
39. Zhang J, Kang B, Tan X, Bai Z, Liang Y, Xing R, et al. Comparative analysis of the protein profiles from primary gastric tumors and their adjacent regions: MAWBP could be a new protein candidate involved in gastric cancer. J Proteome Res. 2007;6:4423–32.
40. Li DM, Zhang J, Li WM, Cui JT, Pan YM, Liu SQ, et al. MAWBP and MAWD inhibit proliferation and invasion in gastric cancer. World J Gastroenterol. 2013;19:2781–92.
41. Li D, Zhang J, Xi Y, Zhang L, Li W, Cui J, et al. Mitogen-activated protein kinase activator with WD40 repeats (MAWD) and MAWD-binding protein induce cell differentiation in gastric cancer. BMC Cancer. 2015;15:637.
42. Long J, Lang ZW, Wang HG, Wang TL, Wang BE, Liu SQ. Glutamine synthetase as an early marker for hepatocellular

carcinoma based on proteomic analysis of resected small hepatocellular carcinomas. Hepatobiliary Pancreat Dis Int. 2010;9:296–305.
43. Li A, Yan Q, Zhao X, Zhong J, Yang H, Feng Z, et al. Decreased expression of PBLD correlates with poor prognosis and functions as a tumor suppressor in human hepatocellular carcinoma. Oncotarget. 2016;7:524–37.
44. Huang S, Li X, Zheng H, Si X, Li B, Wei G, et al. Loss of super-enhancer-regulated circRNA Nfix induces cardiac regeneration after myocardial infarction in adult mice. Circulation. 2019;139:2857–76.